Published in final edited form as:

FASEB J. 2022 August ; 36(8): e22441. doi:10.1096/fj.202101627RR.

The synaptosome-associated protein-23 (SNAP23) is necessary for proper myogenesis

Gabrielle M. Gentile[1,2,#], **Jennifer R. Gamarra**[1,#], **Nichlas M. Engels**[1,#], **R. Eric Blue**[1,#], **Isabel Hoerr**[1], **Hannah J. Wiedner**[1,2], **Emma R. Hinkle**[1,2], **Jessica L. Cote**[1], **Elise Leverence**[1], **Christine A. Mills**[3], **Laura E. Herring**[3], **Xianming Tan**[4,5], **Jimena Giudice**[1,2,6,*]

[1]Department of Cell Biology and Physiology, The University of North Carolina at Chapel Hill, Chapel Hill, NC 27599, USA.

[2]Curriculum in Genetics and Molecular Biology, The University of North Carolina at Chapel Hill, Chapel Hill, NC 27599, USA.

[3]UNC Proteomics Core Facility, Department of Pharmacology, The University of North Carolina at Chapel Hill, Chapel Hill, NC 27599, USA.

[4]Department of Biostatistics, The University of North Carolina at Chapel Hill, Chapel Hill, NC 27599, USA.

[5]Lineberger Comprehensive Cancer Center, The University of North Carolina at Chapel Hill, Chapel Hill, NC 27599, USA.

[6]McAllister Heart Institute, The University of North Carolina at Chapel Hill, Chapel Hill, NC 27599, USA.

Abstract

Vesicle-mediated transport is necessary for maintaining cellular homeostasis and proper signaling. The synaptosome-associated protein-23 (SNAP23) is a member of the SNARE protein family and mediates the vesicle docking and membrane fusion steps of secretion during exocytosis. Skeletal muscle has been established as a secretory organ; however, the role of SNAP23 in the context of skeletal muscle development is still unknown. Here, we show that depletion of SNAP23 in C2C12 mouse myoblasts reduces their ability to differentiate into myotubes as a result of premature cell cycle exit and early activation of the myogenic transcriptional program. This effect is rescued when cells are seeded at a high density or when cultured in conditioned medium from wild

*Corresponding author. Mailing address: Department of Cell Biology and Physiology. The University of North Carolina at Chapel Hill. 6340B Medical Biomolecular Research Building. 111 Mason Farm Rd., Chapel Hill, NC 27599, USA. Telephone number: 1-919-962-6260. jimena_giudice@med.unc.edu.

#These authors contributed equally.

AUTHOR CONTRIBUTIONS

Conceptualization, J.G.; Methodology, L.H., X.T., and J.G.; Investigation, G.M.G., J.R.G., N.M.E., R.E.B., I.H., H.J.W., E.R.H., J.L.C., E.L., L.H., and J.G.; Validation, G.M.G., J.R.G., N.M.E., R.E.B., I.H., H.J.W., E.R.H., J.L.C., E.L., and J.G.; Formal Analysis, G.M.G., J.R.G., N.M.E., R.E.B., I.H., H.J.W., E.R.H., J.L.C., E.L., C.A.M., L.H., X.T., and J.G.; Writing – Original Draft, G.M.G., J.R.G., N.M.E., R.E.B., and J.G.; Writing – Review & Editing, G.M.G., J.R.G., N.M.E., R.E.B., I.H., H.J.W., E.R.H., J.L.C., E.L., C.A.M., L.H., X.T., and J.G.; Visualization, G.M.G., J.R.G., N.M.E., R.E.B., and J.G.; Funding Acquisition, J.G.; Resources, J.G.; Supervision, L.H., J.G.

CONFLICT OF INTEREST

None

type cells. Proteomic analysis of collected medium indicates that SNAP23 depletion leads to a misregulation of exocytosis, including decreased secretion of the insulin-like growth factor 1 (IGF1), a critical protein for muscle growth, development, and function. We further demonstrate that treatment of SNAP23-depleted cells with exogenous IGF1 rescues their myogenic capacity. We propose that SNAP23 mediates the secretion of specific proteins, such as IGF1, that are important for achieving proper differentiation of skeletal muscle cells during myogenesis. This work highlights the underappreciated role of skeletal muscle as a secretory organ and contributes to the understanding of factors necessary for myogenesis.

Keywords

SNAP23; secretion; proliferation; myogenesis; IGF1

INTRODUCTION

The transport of cargo through the endomembrane system modulates cell-cell communication, cell signaling, and intracellular homeostasis. This compartmentalized movement of proteins within membrane-bound vesicles is therefore necessary for maintaining proper cellular physiology. In striated muscles, membrane trafficking is critical for contractile functions, as defects in membrane trafficking contribute to muscular dystrophies, congenital cardiomyopathies, heart failure, and muscle wasting, among several other diseases[1–9].

The transport of cargo from the intracellular to the extracellular space is known as exocytosis. Exocytosis is mediated through docking and subsequent fusion of intracellular vesicles with the plasma membrane, leading to the release of molecules outside of the cell. Key proteins regulate vesicle docking and fusion during secretion, including those belonging to the SNARE (soluble N-ethylmaleimide-sensitive factor attachment protein receptor) family. The core SNARE complex, composed primarily of syntaxins, vesicle-associated membrane proteins (VAMPs, also known as synaptobrevins), and synaptosome-associated proteins (SNAPs), mediates membrane fusion throughout the secretory pathway[10].

Syntaxins and VAMPs are ubiquitously expressed within all cell types; however, SNAP proteins show some cell type-specificity. While SNAP25 is almost exclusively expressed within the brain, SNAP23 is found in all mammalian cells as an essential component of the fusion machinery[11]. The importance of SNAP23 within the trimeric core SNARE complex is further exemplified by the impact of genetic ablation of individual components. Depletion of syntaxin and VAMP proteins in murine models results in no significant impairment of embryonic development[12,13]. Similarly, SNAP25 deletion does not affect embryo viability[14]. In contrast, a global SNAP23 knockout results in pre-implantation embryonic lethality in mice[15].

Modulating SNAP23 expression in a tissue-specific manner has shed light on its role in the physiology of individual organs. Knockout studies in adipocytes[16], the central nervous system[17], and B and T cells[18] have demonstrated that SNAP23 is a key player in the physiology of different organs. Moreover, we know that SNAP23 plays an important role

in trafficking of proteins such as the GLUT4 glucose transporter in adipocytes[19], pancreatic acinar cells[20], and the release of dense core granules in platelets[21,22]. In the context of muscle, however, the characterization of SNAP23 is limited. In skeletal muscle, SNAP23 has been shown to localize to mitochondria and lipid droplets[23]. In atrial myocytes, SNAP23 competes with the SNAP-associated protein (SNAPIN) to interact with the L-type calcium channel CAV1.3, and high concentrations of SNAP23 increased CAV1.3 stability[24]. In patients with atrial fibrillation, CAV1.3 is downregulated, indicating that SNAP23 function might modulate proper electrical signaling in atrial cardiomyocytes[24]. It has also been demonstrated that SNAP23 is responsible for secreting microRNAs from endothelial cells during smooth muscle cell activation in response to shear stress[25].

SNAP23 is constitutively expressed during skeletal muscle cell differentiation (myogenesis); however, identifying the role of SNAP23 in this context remains to be elucidated. Indeed, myogenesis requires the precise trafficking of intracellular and extracellular components[8], and SNARE proteins may play crucial roles. Myogenesis is a complex and dynamic process that is attained in multiple steps. Proliferating myoblasts first exit the cell cycle, thereby committing to differentiation[26,27]. The myoblasts then migrate and align, fusing into long, multinucleated myotubes[28]. These myotubes ultimately mature into fully functional myofibers, which are capable of contraction and force generation[29].

Myoblast proliferation and differentiation are antagonistic muscle cell states[27]; therefore, myogenesis requires cells to strike the proper balance between cell division and cell cycle exit for healthy differentiation. The cell cycle consists of four successive phases: gap 1 (G1), synthesis (S), gap 2 (G2), and mitosis (M). Progression through each of these phases is tightly controlled by cyclin and cyclin-dependent kinase (CDK) proteins. Cyclin expression levels rise and fall throughout the cell cycle, thereby orchestrating the transition from one phase to the next. Myoblasts will proliferate until they are challenged by growth factor deprivation or other external stimuli, which cause the cells to irreversibly withdraw from the cell cycle and undergo differentiation[26].

During myogenesis, the balance between the proliferation and differentiation states of myoblasts is controlled by myogenic regulatory factors (MRFs)[30]. MRFs are transcription factors that activate the myogenic gene expression program to drive muscle cell differentiation[31,32]. Two well-studied MRFs are the myoblast determination protein 1 (MYOD1) and myogenin (MYOG). MYOD1 is expressed in proliferating myoblasts that have committed to the myogenic lineage[30,33], while MYOG acts downstream of MYOD1 as a differentiation factor[30,34,35]. Together, the transcriptional changes induced by the MRFs turn off cell cycle genes and turn on genes involved in mature muscle function, such as the myosin heavy chain (MYH) isoforms, to promote differentiation and contractile properties[35,36].

To migrate, align, and fuse, myoblasts largely rely upon their surrounding niche environment. Skeletal muscle cells are nested within a diverse network of proteins that comprise the extracellular matrix (ECM), including collagens, glycoproteins, and proteoglycans[22,37–39]. It is well-known that the structure of the ECM is important for myogenesis, providing the proper scaffolding and support for cell adhesion, migration, and

fusion[22,37]. Indeed, recent work has shown that collagen, the most abundant component in the ECM, promotes C2C12 cell migration and differentiation[40]. Additionally, the composition of the ECM is dynamically remodeled during skeletal muscle development, allowing the cells to maintain the appropriate physiological state and behavior as they differentiate[22,37–39,41].

Proteomic profiling of skeletal muscle cells has revealed that skeletal muscle is a secretory organ[42–44]. Muscle cells can secrete ECM components as well as enzymes, growth factors, and signaling molecules, which together establish an environment conducive for metabolism, inflammation, proliferation, migration, and differentiation[42–44]. Specifically, the cytokines and peptides produced by myofibers, known as myokines, are necessary for the communication with other organs, the control of muscle hypertrophy, and the regulation of muscle regeneration and maintenance[42,43]. New treatments for muscular diseases would benefit from a greater understanding of the regulation and function of the secretory pathway in skeletal muscle and from the identification of new molecular factors that fine-tune the secretion of myokines into the extracellular milieu.

Here, we investigated the function of SNAP23 in muscle cells. We show that SNAP23 is important for regulating myoblast cell cycle progression and the activation of the myogenic transcriptional program, which together influence the ability of myoblasts to fully differentiate into myotubes. Furthermore, through rescue experiments with conditioned medium along with unbiased secretome studies, we revealed that SNAP23 mediates the exocytosis of the insulin-like growth factor 1 (IGF1). This suggests that SNAP23-mediated secretion of IGF1, and potentially other growth factors, is important for proper skeletal muscle cell proliferation, differentiation, and morphology. Overall, we have revealed a previously unknown role of SNAP23 in the secretion of myokines that regulate myogenesis.

MATERIALS AND METHODS

Cell culture.

Undifferentiated C2C12 myoblasts (ATCC® CRL-1772™) were cultured maintaining low confluency (less than 60%) in Dulbecco's Modified Eagle's Medium (DMEM) supplemented with 10% fetal bovine serum (FBS) (Gemini Bio-Products), 100 units/mL penicillin, and 100 μg/mL streptomycin (referred to as growth medium). To induce myoblast differentiation, cells were grown to high confluence (80–95%), rinsed with PBS (pH 7.4), and cultured in DMEM supplemented with 2% horse serum (Gibco), 100 units/mL of penicillin, and 100 μg/mL streptomycin (referred to as differentiation medium). Cells were maintained in a 37°C humidified incubator in a 5% CO_2 atmosphere.

Delivery of small interfering RNAs (si-RNAs).

C2C12 myoblasts were seeded into six well plates (70,000–100,000 cells per well) in growth medium lacking antibiotics to ensure 50–60% confluence by the next day. Myoblasts were transfected using Lipofectamine RNAiMAX transfection reagent (Invitrogen) and 10 pmol stealth si-RNAs (Invitrogen) (Supplemental Table 1) following the recomended protocol from the manufacturer. When myoblasts reached 80–95% confluence, they were

rinsed with PBS (pH 7.4) and differentiated for four to six days in differentiation medium. Myotubes were rinsed with PBS and processed for immunofluorescence or for RNA or protein extraction.

RNA extraction and reverse transcription.

RNA was extracted using TRIzol reagent (Invitrogen) following the manufacturer's suggested protocol. RNA concentration was measured using a nanodrop lite spectrophotometer (Thermo Fisher Scientific). RNA (2–4 μg) was reversed transcribed into cDNA using the High-Capacity cDNA Reverse Transcription Kit (Applied Biosystems) per the manufacturer's suggested protocol. The reverse transcription thermocycler protocol was as follows: (i) 25°C for 10 min, (ii) 37°C for 120 min, (iii) 85°C for 5 min, (iv) 4°C pause.

Quantitative real-time PCR (qPCR).

Transcripts for Snap23, Ccnd1 (cyclin d1), Igf1, Myh3 (myosin heavy chain 3), Myod1 (myoblast determination protein 1), Myog (myogenin), Ki67, Gapdh (glyceraldehyde-3-phosphate dehydrogenase), Hmbs (hydroxymethylbilane synthase), and Rpl30 (ribosomal protein L30) were evaluated using TaqMan probes (Supplemental Table 2). Reactions containing 50–100 ng cDNA template were performed in quadruplicate using the TaqMan Fast Advanced master mix buffer (Applied Biosystems) and amplified with the StepOnePlus Real-Time PCR system (Applied Biosystems). Relative mRNA expression and fold changes were estimated by applying the delta-delta threshold cycle (ΔΔCt) quantification method using Gapdh, Hmbs or Rpl30 as housekeeping genes. Expression levels were further normalized to mock samples or control luciferase (si-Luc) treated samples.

Protein extraction for western blotting.

C2C12 cells were scraped in RIPA buffer (50 mM Tris pH 7.5, 150 mM NaCl, 5 mM EDTA, 1% Triton X-100, 0.1% SDS, 0.5% sodium deoxycholate) supplemented with Halt protease and phosphatase inhibitors (Thermo Fisher Scientific), incubated on ice for 15–30 min, sonicated, incubated again on ice for 15 min, centrifuged at top speed for 10 min, and frozen. Protein concentration was measured using either a Pierce BCA protein assay kit (Thermo Fisher Scientific) or a Prometheus BCA assay kit (Genesee Scientific) per the manufacturer's suggested protocol for microplates.

Western blot assays.

Protein samples (25–40 μg) or the collected medium were prepared in loading buffer (62.5 mM Tris-HCl pH 7.5, 10% glycerol, 2% SDS, 0.02% bromophenol blue, 143 mM beta-mercaptoethanol) and incubated for 5 min at 95°C before loading into 12% or 4–20% gradient Mini-Protean TGX Stain-Free Gels (BioRad), or 12% long polyacrylamide gels (prepared in-house). Protein samples were electrophoresed in running buffer (25 mM Tris, 190 mM glycine, 0.1% w/v SDS, pH 8.3) for: (a) 30 min at 90 V and then for 60–120 min at 90–120 V (mini gels) or (b) for 60 min at 100 V and then for 4 h at 170 V (long polyacrylamide gels). Protein samples were transferred onto 0.2 μm Amersham Hybond PVDF low fluorescence membranes (Cytiva) for 60 min at 100 V. For total protein visualization, the membranes were stained with Ponceau S solution (Sigma Aldrich, P7170)

for long polyacrylamide gels or exposed to UV light for 2.5–5 min (ChemiDoc XRS+, BioRad) to activate the TGX within the mini gels. Membranes were blocked with 5% non-fat dried milk in Tris-buffered saline (19 mM Tris pH 7.6, 2.7 mM KCl, 137 mM NaCl) containing 0.1% Tween 20 (TBST) for 60 min and incubated overnight at 4°C with the primary antibodies diluted in 5% bovine serum albumin (BSA) in TBST (Supplemental Table 3). The next day, the membranes were washed three times (for 10 min each) with TBST and incubated for 60–90 min in the dark at room temperature with a polyclonal goat anti-rabbit IgG (H+L) secondary antibody DyLight 800 4X PEG (Invitrogen, SA5-35571) or a goat anti-mouse IgG (H+L) secondary antibody DyLight 800 4X PEG (Invitrogen, SA5-35521) diluted 1:10,000 in 5% BSA or 5% milk in TBST. Membranes were then washed three times (for 10 min each) with TBST. Fluorescent signal was detected using the Odyssey CLx Blot Imager (Li-Cor) and analyzed by densitometry. Protein levels were normalized either to a housekeeping gene or total transferred protein (full lanes) visualized by either Ponceau stain (long polyacrylamide gels) or the BioRad ChemiDoc XRS+ system (mini gels).

Confluency assay.

C2C12 myoblasts were transfected as described above. The next day, cells were collected, counted, and re-seeded into six well plates at a range of densities (80,000, 160,000, or 640,000 cells per well). Cells were then cultured in differentiation medium for five days.

Coating of culture plates with fibronectin, gelatin, or collagen.

Six well culture plates were coated with 0.05% gelatin type B (Sigma Aldrich, G1393) for 45 min at 37°C. Alternatively, plates were coated with 0.05 mg/mL PureCol Type I collagen (Advanced BioMatrix, #5005) or 1.58 μg/mL fibronectin and were incubated overnight at 37°C. Plates were then rinsed with PBS (pH 7.4) and dried under UV sterilization.

Collection of conditioned medium.

C2C12 myoblasts were cultured in growth medium until they reached 80–95% confluence. Myoblasts were then differentiated in differentiation medium. The enriched conditioned medium was collected from cultures at days two, four, six, and eight after the initiation of differentiation. The conditioned medium was centrifuged at 1,200 r.p.m. for 5 min and filtered through a 0.2 μm filter before storing separately in frozen stocks.

Treatment of SNAP23-depleted cells with the conditioned medium.

Once the si-RNA transfected myoblasts reached 80–95% confluence, they were rinsed with PBS (pH 7.4). Half of the transfected cells were differentiated with standard differentiation medium. The remainder of the transfected cells were differentiated using conditioned medium. To prepare the conditioned medium, equal parts of standard differentiation medium (DMEM supplemented with 2% horse serum, and antibiotics) and conditioned medium (a mixture of equal volumes of conditioned medium collected from differentiation days two, four, six, and eight) were added together to form the enriched medium. Transfected cells were differentiated for four to six days with daily medium replenishment. Cells were fixed,

rinsed three times with PBS (pH 7.4), and subsequently processed for immunofluorescence experiments.

Treatment of cells with IGF1.

Following the delivery of si-RNAs against the control luciferase reporter or si-Snap23 #2 (MSS209236), myoblasts were maintained in growth medium without antibiotics until they reached 80–95% confluence. Myoblasts were briefly rinsed with PBS (pH 7.4) and differentiated in standard differentiation medium supplemented daily with vehicle (0.1% BSA), 10 ng/mL IGF1, or 1 ng/mL IGF1 (Sigma Aldrich, I3769) for five days. Cells were fixed, rinsed three times with PBS (pH 7.4), and processed for immunofluorescence studies.HHkld;laskfj

Bromodeoxyuridine (BrdU) labeling assay.

Following the delivery of si-RNAs against the control luciferase reporter or si-Snap23 #2 (MSS209236), cells were maintained in growth medium for 24–48 hours. For myoblasts, the cells were treated with 10 μM of BrdU (Abcam, ab142567) for 2 h at 37°C. For myotubes, the cells were first cultured in differentiation medium for four days. Cells were then treated with 10 μM of BrdU for 18 h at 37°C. Following BrdU treatment, cells were washed three times (for 2 min each) with PBS (pH 7.4). Cells were then fixed in 4% paraformaldehyde for 20 min, washed three times (for 10 min each) with PBS (pH 7.4), incubated with 0.5% Triton X-100 for 15 min, and then incubated in blocking solution (1% BSA, 0.3% Triton X-100 in PBS, pH 7.4) for 60 min at room temperature. After blocking, cells were treated with 1.5 M HCl (Fisher Scientific, A144) for 60 min at room temperature to hydrolyze the DNA. The HCl was removed and cells were neutralized with 0.1 M sodium borate (pH 8.5) (Sigma, SX0355) for 30 min at room temperature. Cells were again washed three times (for 10 min each) with PBS (pH 7.4), and then incubated with 4 μg/mL mouse monoclonal (IIB5) anti-BrdU (Santa Cruz Biotechnology, sc-32323) diluted in blocking solution overnight at 4°C. The next day, cells were washed three times (for 10 min each) with PBS (pH 7.4) and incubated with 4 μg/mL goat polyclonal anti-mouse IgG (H+L) Alexa Fluor 488 (Invitrogen, A11001) diluted in blocking solution for 60 min at room temperature and protected from the light. Cells were once again washed three times (for 10 min each) with PBS (pH 7.4) and stained with 2 μM DAPI (Invitrogen, D1306) for 5 min at room temperature. Cells were washed three times (for 5 min each) with PBS (pH 7.4) and then imaged using confocal microscopy.

TUNEL staining.

Coverslips were coated with 0.1 mg/mL Purecol Type I collagen (Advanced BioMatrix, #5005) and were incubated overnight at 37°C. Coverslips were then rinsed with PBS (pH 7.4) and allowed to dry. C2C12 myoblasts were seeded onto the coverslips (100,000 cells per well) and transfected the next day with si-RNAs against the control luciferase reporter or si-Snap23 #2 (MSS209236). For myoblasts, the cells were maintained in growth medium for 48h after transfection. For myotubes, the cells were cultured in differentiation medium for four days. Cells were washed briefly with PBS (pH 7.4), fixed in 4% paraformaldehyde in PBS (pH 7.4) for 15 min at room temperature, permeabilized in 0.5% Triton X-100 in PBS (pH 7.4) for 20 min at room temperature, and washed briefly with deionized H_2O.

As a positive control, cells were incubated with DNase I (Invitrogen, #18068015) for 30 min at room temperature then washed briefly with deionized H_2O. The Click-iT Plus TUNEL Assay kit (Invitrogen, C10617) was used to stain apoptotic cells according to the manufacturer's protocol. Cells were then stained with 2 μM DAPI (Invitrogen, D1306) for 5 min at room temperature. Cells were washed three times (for 5 min each) with 3% BSA in PBS (pH 7.4) and then imaged by confocal microscopy.

Immunofluorescence assays.

Cells were washed briefly with PBS (pH 7.4), fixed in 2–4% paraformaldehyde in PBS (pH 7.4) for 30 min, washed three times (for 10 min each) with PBS (pH 7.4) (for 10 min each), and then incubated in blocking solution (1% BSA, 0.3% Triton X-100 in PBS (pH 7.4)) for 60 min at room temperature. Cells were then incubated with 4 μg/mL mouse monoclonal (B-5) anti-MYH3 (Santa Cruz Biotechnology, sc-376157) diluted in blocking solution overnight at 4°C. The following day, cells were washed three times (for 10 min each) with PBS (pH 7.4) and incubated with 4 μg/mL goat polyclonal anti-mouse IgG (H+L) Alexa Fluor 488 (Invitrogen, A11001) diluted in blocking solution for 60–90 min at room temperature and protected from the light. Cells were once again washed three times (for 10 min each) with PBS (pH 7.4) and stained with 2–3 μM DAPI (Invitrogen, D1306) for 5 min at room temperature. Cells were washed three times (for 5 min each) with PBS (pH 7.4) and then imaged using confocal microscopy.

Confocal microscopy.

The Hooker Imaging Core at The University of North Carolina at Chapel Hill provided access to a Zeiss LSM 880 confocal microscope with a 10x Plan Apochromat objective (0.45 WD) (for six well plates) or 63x Oil Immersion objective (for coverslips). Laser excitation was as follows: argon multiline laser at 488 nm (Alexa Fluor 488) (2% power) or a 405 nm diode at 30 mW (DAPI) (2% power). Emission filters for all experiments were set as follows: 490–615 nm (Alexa Fluor 488) and 410–514 nm (DAPI). A tile scan of nine frames (1,024 × 1,024 pixels per frame, 10% overlap) was taken for each treatment condition and the nine frames were stitched together using ZEN black imaging software (Zeiss).

Image processing and quantitation.

Processing and quantitative analysis of confocal images were performed using ImageJ software (imagej.nih.gov) and MyoCount (version 1.3.1). For MyoCount, each image was first divided into nine panels (3 × 3 grid). The images were then processed using MyoCount as previously described[45] with optimized parameter settings based on the average image area occupied by myotubes (Supplemental Tables 4 and 5). The fusion index was estimated as the ratio between the number of nuclei in MYH3-positive cells with more than two nuclei and the total number of nuclei in a field of view. The myotube diameter was estimated by measuring the size of three lines that were drawn perpendicular to the myotube longitudinal axis. The average of three measurements per myotube was then calculated. Myotube length was estimated by measuring the size of a line that was drawn parallel to the myotube longitudinal axis. The average of measurments for all myotubes analyzed in the field of view

was then calculated. Only full myotubes in the images were used for this analysis. Myotubes that were incomplete (*i.e.*, cut off by the border of the images) were not analyzed.

Collection of secretome medium for mass spectrometry studies.

C2C12 were transfected with si-RNAs against the control luciferase reporter or si-Snap23 #2 (MSS209236). Cells were maintained in growth medium in 10 cm culture plates until they reached 80–95% confluence. Cells were then differentiated in differentiation medium. Three days after the initiation of differentiation, cells were rinsed with PBS (pH 7.4) and the medium was replaced with 7 mL of serum-free, phenol-free DMEM (Thermo Fisher Scientific, #21063–029). The next day, the medium was collected (day four of differentiation) and replenished with 7 mL of serum-free, phenol-free DMEM. On day six of differentiation, the medium was again collected. Equal volumes of medium collected on day four and day six were combined for each treatment condition. The medium was passed through a 0.22 μm polyethersulfone (PES) filter for sterilization. The medium was concentrated to a final volume of 100–200 μL using an Amicon Ultra-4 filter (Millipore, UFC800324). In brief, filters were first rinsed with 1N NaOH (1 mL). Filters were washed by adding 1 mL of PBS (pH 7.4) and then spinning at 4,000 × g for 5 min. Medium was added to the filter in 1 mL increments followed by spinning at 4,000 × g for 10 min until the final concentrated volume was reached.

Sample preparation for proteomics analysis.

The secretome protein samples (100 μg per replicate, n=3) were treated with 8 M urea, then reduced with 5 mM dithiothreitol for 30 min and alkylated with 15 mM iodoacetamide for 45 min. The samples were then digested at a 1:50 protease:protein ratio with LysC (Wako) for 2 h at 37°C, diluted to 1 M urea, then digested with MS grade trypsin (Promega) at 37°C overnight. The peptide samples were acidified to 1% trifluoroacetic acid, then desalted using Peptide Desalting Spin Columns (Pierce Thermo Fisher Scientific). The samples were dried via vacuum centrifugation, then resuspended in 0.1% formic acid for BCA fluorometric peptide quantitation assay (Pierce).

Liquid chromatography with tandem mass spectrometry (LC-MS/MS) analysis.

Samples were normalized and 0.6 μg of each sample was analyzed by LC-MS/MS using an Easy nLC 1200 coupled to a Fusion Lumos (Thermo Fisher Scientific). Samples were injected onto an Easy Spray PepMap C18 column (75 μm id × 25 cm, 2 μm particle size) (Thermo Fisher Scientific) and separated over a 120 min method. The gradient for separation consisted of 5-32-45% mobile phase B at a 250 nL/min flow rate, where mobile phase A was 0.1% formic acid in water and mobile phase B consisted of 0.1% formic acid in 80% acetonitrile. Fusion Lumos was operated in data-dependent mode with a 3 s cycle time. Resolution for the precursor scan (m/z 350–1500) was set to 120,000 with a 250% AGC target, 50 ms inject time. MS/MS scans acquired in the Orbitrap with a resolution set to 15,000, 250% AGC target, 50 ms inject time. The normalized collision energy was set to 30% for higher energy collisional dissociation (HCD), with an isolation window of 1.6 m/z. MIPS was on, and precursors with unknown charge or a charge state of 1 and ≥ 7 were excluded.

MS data analysis.

Raw data files were processed using MaxQuant version 1.6.15.0 and searched against a reviewed Uniprot mouse database (containing 17,457 sequences) using Andromeda within MaxQuant. Enzyme specificity was set to trypsin, up to two missed cleavage sites were allowed, carbamidomethylation of cysteine was set as a fixed modification, and oxidation of methionine and acetyl of protein-N terminus were set as variable modifications. Label-free quantification (LFQ) using razor + unique peptides was enabled. Match between runs was enabled with a matching time window of 0.7 min. A 1% false discovery rate (FDR) was used to filter all data. Additional analysis was performed in Perseus[46]. A minimum of 2 unique+razor peptides per protein and > 50% non-zero values across the datasets were required for quantification. Imputation of missing values based on normal distribution with width of 0.3 and downshift of 1.8, was performed. Student's T-test was performed for each pairwise comparison and *p*-values were calculated. A LFQ fold change ratio for each pairwise comparison was calculated. Differentially secreted proteins were filtered from the MS data based on the following criteria: fold change ≥ 1.5 and $p \leq 0.05$. The Database for Annotation, Visualization, and Integrated Discovery (DAVID) was used for Gene Ontology (GO) and Functional Annotation analysis of the differentially secreted proteins.

Statistical analysis.

Proteomics statistical analysis is described above. For all other analyses, differences between control and treatment groups were determined using one-way or two-way ANOVA with Bonferroni post hoc test for multiple comparisons, or an upaired Student's T-test (two-tailed). For nuclei per myotube analysis, we employed a one-way multi-variate analysis of variance (MANOVA) accompanied by Pillai's trace as the test statistical reference. Statistical analysis was performed using Microsoft Excel (Microsoft), R (version 4.0.3 R Core Team 2020), or GraphPad Prism 5, version 5.0f (GraphPad Software Inc.). Statistical significance was verified if $p \leq 0.05$. All data are represented as mean ± SEM from at least three independent experiments.

RESULTS

SNAP23 is required for myoblast differentiation into elongated myotubes

To investigate the functions of SNAP23, we first assessed SNAP23 protein levels during myogenesis. A C2C12 time-course analysis revealed that SNAP23 is expressed at comparable levels throughout muscle cell differentiation (Supplemental Fig. S1A). The appearance of a second SNAP23 band during the differentiation time-course is consistent with previous studies reporting that Snap23 mRNA is alternatively spliced in heart and skeletal muscle tissues[47,48]. We then depleted Snap23 mRNA by delivering si-RNAs in C2C12 mouse myoblasts prior to induction of cell differentiation. Western blot and qPCR assays confirmed effective knockdown of the SNAP23 isoforms in myoblasts (Supplemental Fig. S1B) and myotubes (Supplemental Fig. S1C). Using immunofluorescence staining for MYH3, a marker of muscle cell differentiation, we observed that SNAP23 depletion led to a reduction in the total number of cells and a less differentiated phenotype when compared to controls (Fig. 1A). Quantification of the microscopy images confirmed our qualitative observations showing a ~46–56% reduction in the number of nuclei per unit area (Fig.

1B), a ~24–47% reduction in the fusion index (Fig. 1C), an increase in the number of myotubes with 2–5 nuclei, and a concomitant reduction of myotubes with >10 nuclei in SNAP23-depleted cells in comparison with controls (Fig. 1D). Additionally, there was a reduction in the average myotube length in the SNAP23 knockdown cells compared to the control cells (Fig. 1E), without significant changes in myotube diameter (Fig. 1F). These data indicate that SNAP23 is required for proper myogenesis, leading us to identify the stage(s) of differentiation being affected.

SNAP23 depletion decreases muscle cell proliferation

The reduction in total nuclei per unit area observed in SNAP23-depleted cells (Fig. 1B) prompted us to determine the effect of SNAP23 depletion on the first step of myogenesis, which is cell cycle exit. We labeled both myoblasts and myotubes with BrdU, a thymidine analog that is incorporated into the DNA of actively replicating cells during S phase of the cell cycle. We observed a significant, 2-fold reduction in BrdU-positive cells upon depletion of SNAP23 in myoblasts (Fig. 2A, *left*). In myotubes, however, there were few cycling cells in either treatment condition (Fig. 2A, *right*). We confirmed these results by performing qPCR assays to measure the levels of Ki67, a marker of cell proliferation that is highly expressed in cells that are in M phase. We found that Ki67 mRNA levels were significantly downregulated in both myoblasts and myotubes that were depleted of SNAP23 (Fig. 2B). The progression of cells from G1 to S phase is controlled by cyclin D1 (CCND1), and the downregulation of CCND1 during myogenesis is a hallmark of muscle cells that have committed to differentiation[49,50]. We therefore assessed the levels of CCND1 in SNAP23-depleted cells. Western blot assays revealed that SNAP23-depleted cells have elevated CCND1 levels, with myotubes exhibiting an ~2-fold upregulation of CCND1 protein expression (Fig. 2C–D).

In addition to a reduction in cell proliferation, the decrease in the total number of nuclei per unit area observed in SNAP23-depleted cells could also be attributed to an activation of apoptosis. To explore this possibility, we performed a TUNEL assay to assess the amount of cell death in myoblasts and myotubes depleted of SNAP23. We did not observe TUNEL-positive cells in either the si-Luc or si-Snap23 condition for myoblasts or myotubes (Supplemental Fig. S2), suggesting that apoptosis does not contribute to the reduced cell number in SNAP23-depleted cells. As a positive control, we treated cells with DNase I to induce DNA strand breaks, and we indeed observed TUNEL-stained nuclei in both conditions for myoblasts and myotubes (Supplemental Fig. S2).

Taken together, our results indicate that SNAP23 is necessary for regulating cell cycle progression and maintaining the proliferative state of myoblasts.

Loss of SNAP23 activates myogenic marker expression in myoblasts

We next asked whether loss of SNAP23 altered the temporal expression of critical myogenic markers. We probed both myoblasts and myotubes for MYOD1 and MYOG, as well as MYH3, a downstream target of MYOG transcriptional control[35]. Surprisingly, we observed a significant upregulation of MYH3 and MYOG at both the mRNA and protein levels in SNAP23-depleted myoblasts relative to the controls (Fig. 3A–C). There was no change,

however, in expression of these myogenic markers in differentiated myotubes (Fig. 3D–F). These results are evidence of an earlier activation of the myogenic transcriptional program and are consistent with the reduced proliferation of SNAP23-depleted myoblasts (Fig. 2A–B).

Given that SNAP23-depleted myoblasts cultured in growth medium appear to be exiting the cell cycle and have turned on the myogenic transcriptional program, exhibiting two signatures of cells committed to the myogenic fate, it was interesting that these cells were not fusing to form fully differentiated myotubes (Fig. 1A). This phenotype could be attributed to an insufficient number of cells at the onset of differentiation, a defect in cell adhesion and cell fusion, or both. We therefore reasoned that by seeding SNAP23-depleted cells at a high density, we could asses whether the decreased number of nuclei per unit area (Fig. 1B) was the cause of the reduced differentiation. Indeed, when SNAP23-depleted myoblasts were seeded at a high confluence (*e.g.*, 160,000 or 640,000 cells per well), the defect in cell fusion and myotube formation was restored (Supplemental Fig. S3).

Collectively, these data suggest that SNAP23-depleted cells fail to fully differentiate due to the combined premature cell cycle withdrawal and activation of myogenic expression programs, which prevents the cells from reaching the proper density necessary for fusion.

Collagen and gelatin coating promotes myogenesis of SNAP23-depleted cells

Since SNAP23 is a member of the SNARE secretory machinery[11], we hypothesized that its depletion in muscle cells would alter the secretion of proteins that participate in autocrine and paracrine signaling programs important for differentiation. Previous reports have characterized the secretome of wild type C2C12 cells and suggested that secreted ECM proteins contribute to cell integrity, growth, differentiation, and regeneration[41,51,52].

We thus repeated the Snap23 knockdown assays on plates coated with either gelatin or collagen (Fig. 4). On uncoated plates, we again observed a defect in differentiation (Fig. 4A, *top row*) and a significant reduction in both the number of nuclei and the fusion index in SNAP23-depleted cells compared to controls (Fig. 4B–C). For two si-RNA treatments, culturing cells on gelatin or collagen rescued the cellular phenotype observed after depletion of SNAP23 (si-Snap23 #2 and #3, Fig. 4A). The phenotype severity was only mildly attenuated for si-Snap23 #1 (Fig. 4A), which was the condition that caused the strongest defect in fusion (Fig. 1C). In comparison with cells cultured on uncoated plastic plates, the number of nuclei per unit area was increased (Fig. 4B) and the fusion index was also rescued (Fig. 4C) when SNAP23-depleted cells were cultured on coated plates.

Given the role of the ECM in enhancing cell adhesion to promote myogenesis, it is possible that the positive effects on differentiation observed when cells are cultured on collagen-coated plates is independent of SNAP23 function. To determine whether SNAP23 depletion affects cell adhesion, we seeded SNAP23-depleted myoblasts on plates coated with collagen, and calculated the total number of nuclei per unit area as a readout of adhered cells. In general, culturing myoblasts on coated plates significantly enhanced cell adhesion to the dish relative to cells cultured on uncoated plates (Fig. 4D, compare no coating to fibronectin and collagen coatings). While there was no difference in the total number of

nuclei between control and si-Snap23 depleted cells seeded on plates coated with fibronectin (Fig. 4D, *middle*), we observed an increase in the ability of SNAP23-depleted cells to adhere to collagen when compared to control cells plated on the same substrate (Fig. 4D, *right*). This supports our previous finding, where culturing cells on collagen-coated plates rescued the total number of nuclei per unit area in differentiated cells (Fig. 4B).

Our results indicate that SNAP23-depleted myoblasts retain the ability to adhere to the ECM and suggest that SNAP23 is mediating the secretion of some other protein(s) critical for muscle cell differentiation.

SNAP23 mediates the secretion of factors that are necessary for myogenesis

Our data led us to ask whether the phenotype observed in SNAP23-depleted cells was rescuable by the secreted factors of wild type cells. We thus evaluated whether medium collected from wild type myotubes (conditioned medium) had the capacity to rescue the reduced total nuclei and fusion phenotypes observed in SNAP23-depleted cells (Fig. 1B–C). We hypothesized that the conditioned medium would contain proteins secreted by healthy cells during myogenesis that serve to promote differentiation.

To test this hypothesis, control and si-Snap23 treated cells were cultured either with regular differentiation medium (Fig. 5A, *top panels*) or with a combination of 50% regular differentiation medium and 50% conditioned medium (Fig. 5A, *bottom panels*). Immunofluorescence staining for MYH3 and DAPI showed a clear rescue of differentiation when SNAP23-depleted cells were cultured using conditioned medium (Fig. 5A, compare top panels with bottom panels). Quantitively, the knockdown cells treated with conditioned media exhibited an increase in total nuclei number and fusion index, nearly matching the control levels (Fig. 5B–C).

This evidence led us to conclude that during myogenesis, control cells secrete specific proteins into the extracellular environment that are important for maintaining proper cell morphology and survival.

SNAP23 depletion influences the secretome profile of muscle cells

We next sought to identify the specific proteins important for myogenesis that are secreted via SNAP23-mediated exocytosis. We therefore analyzed the differentiation medium from SNAP23-depleted myotubes and wild type myotubes by mass spectrometry-based proteomics.

We identified 112 differentially secreted proteins (≥ 1.5-fold change, $p \leq 0.05$) between the SNAP23-depleted and control samples (Fig. 6A) (Supplemental Data File 1). Of these, 55 proteins were downregulated (secreted less by SNAP23-depleted cells than by controls) (Supplemental Table 6 and Fig. 6B, *red*) and 57 were upregulated (secreted more by SNAP23-depleted cells than by controls) (Supplemental Table 7 and Fig. 6B, *blue*). GO analysis of these subsets revealed that 67 out of the 112 (60%) of the differentially secreted proteins were known residents of the extracellular space (Fig. 6C). Further analysis of the associated GO biological processes revealed an enrichment in categories related with

cell-cell adhesion for the downregulated proteins (Fig. 6D, *top*) and muscle contraction for the upregulated proteins (Fig. 6D, *bottom*).

Collectively, our unbiased analysis indicates that the phenotyes observed in SNAP23-depleted cells could be driven by a reduced abundance of proteins secreted into the extracellular space that function to mediate the communication within and between cells during myogenesis.

IGF1 secretion is reduced upon SNAP23 depletion and its exogenous addition rescues cellular myogenic capacity

One interesting candidate identified from the proteomics study was IGF1 (Fig. 6A, *in red*). IGF1 is a well-known regulator of myogenesis, activating downstream signaling pathways that converge to promote cell proliferation and differentiation[53]. In our proteomics analysis, we found that IGF1 levels were reduced in the medium collected from SNAP23-depleted C2C12 cells (0.4-fold change, $p = 0.03$) (Supplemental Table 6). We validated by western blot that IGF1 was indeed reduced in the medium from SNAP23-depleted cells (Fig. 7A). Importantly, the total Igf1 mRNA expression was not significantly different between the SNAP23-depleted cells and controls (Fig. 7B). This suggests that IGF1 secretion is not reduced by its intracellular production but rather by the loss of SNAP23.

The silencing of certain SNARE proteins, such as SNAP23, in neurons has been previously reported to repress axon growth and polarization by inhibiting the exocytic transport of the IGF1 receptor[54]. Exogenous treatment of neurons with IGF1 recruited SNAP23, in conjunction with other SNARE proteins, to associate with vesicles containing the IGF1 receptor[54]. We thus asked whether adding exogenous IGF1 would stimulate SNAP23-depleted cells to recover their myogenic capacity. When differentiation medium was supplemented with either 1 ng/mL or 10 ng/mL IGF1, we observed a rescue in the total number of nuclei and in the overall differentiation of SNAP23-depleted cells (Fig. 7C–D).

These data led us to conclude that SNAP23 mediates the secretion of IGF1 from muscle cells to the extracellular space, where IGF1 contributes to differentiation of myoblasts into multinucleated myotubes.

DISCUSSION

Skeletal muscle is known to be impacted by extracellular factors such as hormones, growth factors, and cytokines to regulate cell proliferation, extracellular matrix remodeling, and migration. Recently, it has been appreciated that muscle cells can secrete myokines to exert either autocrine, paracrine, or endocrine effects[42,43]. While the SNARE proteins have been extensively studied in the context of fusing synaptic vesicles, very little is known about their roles and regulation in striated muscles. Our study aimed to address this gap of knowledge by identifying the role of the secretory-mediating protein SNAP23 in skeletal muscle cells.

We demonstrated that SNAP23 is necessary for muscle cell proliferation and proper differentiation. When SNAP23 was depleted in C2C12 cells, we observed a decrease in total cell number and in fusion index, as well as an increase in the number of small myotubes

(those containing 2–5 nuclei) and a reduction in the average myotube length (Fig. 1). We found this phenotype to be a consequence of reduced cell proliferation in SNAP23-depleted myoblasts (Fig. 2A–B) rather than an activation of apoptosis (Supplemental Fig. S2). These data suggest that the impaired myotube formation observed in SNAP23-depleted cells is a result of insufficient cell number at the onset of differentiation.

The switch from the proliferating to the differentiating cell state is known to be initiated by cell-cell contact inhibition[55–57]. Muscle cells need to reach a threshold confluency before they are activated to fuse, and this cell-cell communication is necessary for turning off the transcription of genes that promote proliferation and turning on the expression of myogenic genes[58,59]. Consistent with the function of CCND1 as a cell cycle regulator, the upregulation of CCND1 (Fig. 2C–D) could indicate a response whereby SNAP23-depleted cells re-enter the cell cycle and start proliferating to increase confluency[60]. CCND1 has also been reported to have cell cycle-independent functions, with increasing evidence implicating CCND1 in migration[61–64]. Consistent with this model, the increased expression of CCND1 in the absence of SNAP23 could evidence cells attempting to migrate in search of a high density environment that is optimal for differentiation.

We further found that SNAP23-depleted myoblasts exhibit a premature expression of myogenic markers (Fig. 3). Interestingly, CCND1 has been implicated in negatively regulating MYOD1 function and differentiation[50,65,66]. While CCND1 is known to promote the G1/S phase transition of the cell cycle, MYOD1 acts antagonistically to block this transition and induce growth arrest[65,67–69]. Previous work has also shown that overexpression of MYOG in proliferating myoblasts resulted in cell cycle exit[34]. It is thus possible that SNAP23-depleted myoblasts are lacking the proper signal to maintain the proliferative state, resulting in the premature cell cycle exit (Fig. 2A–B) and concomitant myogenic marker expression (Fig. 3). Furthermore, when SNAP23-depleted cells are challenged by growth factor withdrawal upon the onset of differentiation, the cells are unable to properly differentiate due to a insufficient number of cells and thus make an effort to compensate by increasing CCND1 expression.

We discovered that when SNAP23-depleted cells were seeded at a higher confluency, the differentiation phenotype was rescued (Supplemental Fig. S3). Further, when SNAP23-depleted cells were plated in conditions of an enhanced extracellular environment, the cells had a significant recovery in the total number of nuclei per unit area and a significant increase in the fusion index (Fig. 4). The enhanced adhesion and restored fusion of SNAP23-depleted cells when cultured on collagen-coated plates is consistent with previous work showing that collagen promotes myogenic migration and differentiation of C2C12 cells[40]. The importance of collagen for cellular differentiation is further highlighted by the fact that collagen is a widely used substrate for coating plates to promote cell adhesion in culture. These results indicate that the ability of myoblasts to fuse and the effect of collagen on myogenesis are both independent from SNAP23 function. This is further supported by the fact that collagen was not observed in the proteomics experiment. Rather, SNAP23 is mediating the secretion of important proteins to maintain the appropriate cell density prior to muscle cell differentiation.

Our experiments with conditioned medium (Fig. 5) were a proxy to validate that SNAP23 is mediating the secretion of a protein or multiple proteins that might be vital to proper myogenesis. We undertook an unbiased approach by performing a secretome analysis to determine which specific proteins are released from muscle cells via SNAP23-mediated secretion. Consistent with the role of SNAP23 as part of the secretory machinery, we observed numerous proteins that were differentially secreted between SNAP23-depleted cells and controls (Fig. 6). Notably, the majority of the differentially secreted proteins were reduced in the conditioned medium of SNAP23-depleted cells compared to the control cells, suggesting that SNAP23 is promoting their secretion.

IGF1 was among the top hits in our secretome study. It has long been known that IGF1 levels increase during myogenesis, and that IGF1 plays essential roles in muscle regeneration and hypertrophy[41,70]. The pathway and proteins that mediate the release of IGF1 into the extracellular milieu of skeletal muscle cells, however, are not well characterized. We validated that SNAP23 mediates the secretion of IGF1 and that this exocytic event is important for myogenesis (Fig. 7). Interestingly, IGF1 has been shown to exhibit a dual function in muscle cells, where IGF1 signaling can promote both proliferation and differentiation after acute and chronic stimulation, respectively[71]. The reduced cell proliferation and the upregulation of MYOG expression in SNAP23-depleted myoblasts supports the established role of IGF1 signaling in enhancing expression of cell cycle genes (*e.g.*, CCND1) and suppressing myogenic markers during initial IGF1 exposure[71]. Furthermore, the loss of differentiation and the upregulation of CCND1 phenotypes observed in SNAP23-depleted myotubes is consistent with the role of chronic IGF1 signaling as a stimulator of myogenesis through the activation of myogenic factors (*e.g.*, MYOG) and the suppression of CCND1 expression[71,72].

Our identification of SNAP23 as a new regulator of IGF1 secretion greatly enhances our understanding of skeletal muscle as a secretory organ. We thus propose a model whereby SNAP23 mediates the release of IGF1 to the extracellular space in muscle cells. Intracellularly, IGF1 signaling synergizes with other competence factors to regulate cell cycle progression and differentiation throughout myogenesis. Future studies will seek to determine the signaling pathway that connects IGF1 secretion to transcriptional regulation.

Supplementary Material

Refer to Web version on PubMed Central for supplementary material.

ACKNOWLEDGMENTS

We acknowledge the support of the Genetics and Molecular Biology Curriculum (GMB), the Program in Translational Medicine, the Mechanistic and Interdisciplinary Biology (MiBio) Graduate Training Program, and the Postbaccalaureate Research Education Program (PREP), all at The University of North Carolina at Chapel Hill. We thank the Hooker Microscopy Core at The University of North Carolina at Chapel Hill where microscopy imaging has taken place and Dr. Robert Currin for training and educating in the use of their equipment.

This work was supported by the following funding sources: start-up funds (Giudice), a Junior Faculty Development Award (Giudice), a Pilot & Feasibility Research Grant (P30-DK056350) (Nutrition and Obesity Research Center) (Giudice), and a Jefferson Pilot Award (Giudice), all from The University of North Carolina at Chapel Hill, the National Institutes of Health (NIH) (NIGMS R01GM130866) (Giudice), a Basil O'Connor Starter Scholar Award (5-FY18-36) from the March of Dimes Foundation (Giudice), and a Career Development Award from the American

Heart Association (19CDA34660248) (Giudice). Gabrielle M. Gentile was supported by a NIH-NIGMS training award (T32GM119999) and by the Graduate Research Fellowship Program (DGE-1650116) from the National Science Foundation (NSF). Hannah J. Wiedner was supported by a merit-doctoral fellowship from the Graduate School at The University of North Carolina at Chapel Hill, a NIH-NIGMS training award (T32GM119999), and by the NSF Graduate Research Fellowship Program (DGE-1650116). Emma R. Hinkle was supported by a NIH-NIAMS F31 predoctoral fellowship (AR077381-01A1) and a NIH-NIGMS training award (5T32GM007092). Jennifer R. Gamarra was supported by a training award from the NIH-NIGMS (R25GM089569). The proteomics studies were conducted at the UNC Proteomics Core Facility, which is supported in part by a P30 CA016086 Cancer Center Core Support Grant to the Lineberger Comprehensive Cancer Center at The University of North Carolina at Chapel Hill. The content is solely the responsibility of the authors and does not necessarily represent the official views of the funding agencies.

DATA AVAILABILITY

The data that support the findings of this study are available in the Materials and Methods section as well as in the Supplemental Material of this article.

NONSTANDARD ABBREVIATIONS

ACTA1	skeletal muscle actin alpha 1
BSA	bovine serum albumin
CAV1.3	calcium channel, voltage-dependent, L type, alpha 1D
CCND1	cyclin D1
CDK	cyclin-dependent kinase
DAVID	database for annotation, visualization, and integrated discovery
ECM	extracellular matrix
GLUT4	glucose transporter type 4
GO	gene ontology
HMBS	hydroxymethylbilane synthase
IGF1	insulin-like growth factor 1
LC-MS/MS	liquid chromatography with tandem mass spectrometry
MYH	myosin heavy chain
MYL	myosin light chain
MYOD1	myoblast determination protein 1
MYOG	myogenin
RIPA	radioimmunoprecipitation assay buffer
RPL30	ribosomal protein L30
SNAP	synaptosome-associated protein

SNAPIN	SNAP-associated protein
SNARE	soluble N-ethylmaleimide-sensitive factor attachment protein receptor
TUBB2B	beta-tubulin
VAMP	vesicle-associated membrane protein
VCAM1	vascular cell adhesion molecule 1

REFERENCES

1. Howell GJ, Holloway ZG, Cobbold C, Monaco AP, Ponnambalam S. Cell biology of membrane trafficking in human disease. Int Rev Cytol. 2006;252:1–69. doi:10.1016/S0074-7696(06)52005-4 [PubMed: 16984815]
2. Bitoun M, Maugenre S, Jeannet PY, et al. Mutations in dynamin 2 cause dominant centronuclear myopathy. Nat Genet. 2005;37(11):1207–1209. doi:10.1038/ng1657 [PubMed: 16227997]
3. D'Alessandro M, Hnia K, Gache V, et al. Amphiphysin 2 Orchestrates Nucleus Positioning and Shape by Linking the Nuclear Envelope to the Actin and Microtubule Cytoskeleton. Dev Cell. 2015;35(2):186–198. [PubMed: 26506308]
4. Lee E, Marcucci M, Daniell L, et al. Amphiphysin 2 (Bin1) and T-tubule biogenesis in muscle. Science. 2002;297(5584):1193–1196. [PubMed: 12183633]
5. Fu Y, Hong TT. BIN1 regulates dynamic t-tubule membrane. Biochimica et Biophysica Acta - Molecular Cell Research. 2015.
6. Böhm J, Vasli N, Maurer M, et al. Altered splicing of the BIN1 muscle-specific exon in humans and dogs with highly progressive centronuclear myopathy. PLoS Genet. 2013;9(6):e1003430. doi: 10.1371/journal.pgen.1003430. doi:10.1371/journal.pgen.1003430 [PubMed: 23754947]
7. Fugier C, Klein AF, Hammer C, et al. Misregulated alternative splicing of BIN1 is associated with T tubule alterations and muscle weakness in myotonic dystrophy. Nat Med. 2011;17(6):720–725. doi:10.1038/nm.2374 [PubMed: 21623381]
8. Towler MC, Kaufman SJ, Brodsky FM. Membrane traffic in skeletal muscle. Traffic. 2004;5(3):129–139. doi:10.1111/j.1600-0854.2003.00164.x [PubMed: 15086789]
9. Dowling JJ, Gibbs EM, Feldman EL. Membrane traffic and muscle: lessons from human disease. Traffic. 2008;9(7):1035–1043. doi:10.1111/j.1600-0854.2008.00716.x [PubMed: 18266915]
10. Jahn R, Scheller RH. SNAREs - Engines for membrane fusion. Nat Rev Mol Cell Biol. 2006;7(9):631–643. doi:10.1038/nrm2002 [PubMed: 16912714]
11. Ran VR, Chawla A, Roche PA. Identification of a novel syntaxin- and synaptobrevin/VAMP-binding protein, SNAP-23, expressed in non-neuronal tissues. J Biol Chem. 1996. doi:10.1074/jbc.271.23.13300
12. Fujiwara T, Mishima T, Kofuji T, et al. Analysis of Knock-Out Mice to Determine the Role of HPC-1/Syntaxin 1A in Expressing Synaptic Plasticity. J Neurosci. 2006;26(21):5767–5776. doi:10.1523/JNEUROSCI.0289-06.2006 [PubMed: 16723534]
13. Schoch S, Deák F, Königstorfer A, et al. SNARE function analyzed in synaptobrevin/VAMP knockout mice. Science. 2001;294(5544):1117–1122. doi:10.1126/SCIENCE.1064335 [PubMed: 11691998]
14. Washbourne P, Thompson PM, Carta M, et al. Genetic ablation of the t-SNARE SNAP-25 distinguishes mechanisms of neuroexocytosis. Nat Neurosci. 2002;5(1):19–26. doi:10.1038/nn783 [PubMed: 11753414]
15. Suh YH, Yoshimoto-Furusawa A, Weih KA, et al. Deletion of SNAP-23 results in pre-implantation embryonic lethality in mice. PLoS One. 2011;6(3):e18444. doi:10.1371/journal.pone.0018444 [PubMed: 21479242]

16. Feng D, Amgalan D, Singh R, et al. SNAP23 regulates BAX-dependent adipocyte programmed cell death independently of canonical macroautophagy. J Clin Invest. 2018;128(9):3941–3956. doi:10.1172/JCI99217 [PubMed: 30102258]
17. Kunii M, Noguchi Y, Yoshimura S, et al. SNAP23 deficiency causes severe brain dysplasia through the loss of radial glial cell polarity. J Cell Biol. 2021;220(1):e201910080. doi:10.1083/JCB.201910080 [PubMed: 33332551]
18. Kaul S, Mittal SK, Feigenbaum L, Kruhlak MJ, Roche PA. Expression of the SNARE protein SNAP-23 is essential for cell survival. PLoS One. 2015. doi:10.1371/journal.pone.0118311
19. Rea S, Martin L, McIntosh S, et al. Syndet, an adipocyte target SNARE involved in the insulin-induced translocation of GLUT4 to the cell surface. J Biol Chem. 1998;273(30):18784–18792. doi:10.1074/JBC.273.30.18784 [PubMed: 9668052]
20. Kunii M, Ohara-Imaizumi M, Takahashi N, et al. Opposing roles for SNAP23 in secretion in exocrine and endocrine pancreatic cells. J Cell Biol. 2016. doi:10.1083/jcb.201604030
21. Williams CM, Li Y, Brown E, Poole AW. Platelet-specific deletion of SNAP23 ablates granule secretion, substantially inhibiting arterial and venous thrombosis in mice. Blood Adv. 2018;2(24):3627–3636. doi:10.1182/BLOODADVANCES.2018023291 [PubMed: 30573565]
22. Csapo R, Gumpenberger M, Wessner B. Skeletal Muscle Extracellular Matrix – What Do We Know About Its Composition, Regulation, and Physiological Roles? A Narrative Review. Front Physiol. 2020. doi:10.3389/fphys.2020.00253
23. Strauss JA, Shaw CS, Bradley H, et al. Immunofluorescence microscopy of SNAP23 in human skeletal muscle reveals colocalization with plasma membrane, lipid droplets, and mitochondria. Physiol Rep. 2016. doi:10.14814/phy2.12662
24. Sun XL, fang Yuan J, Jin T, et al. Physical and functional interaction of Snapin with Cav1.3 calcium channel impacts channel protein trafficking in atrial myocytes. Cell Signal. 2017;30:118–129. doi:10.1016/j.cellsig.2016.11.019 [PubMed: 27915047]
25. Zhu JJ, Liu YF, Zhang YP, et al. VAMP3 and SNAP23 mediate the disturbed flow-induced endothelial microRNA secretion and smooth muscle hyperplasia. Proc Natl Acad Sci U S A. 2017;114(31):8271–8276. doi:10.1073/pnas.1700561114 [PubMed: 28716920]
26. Walsh K, Perlman H. Cell cycle exit upon myogenic differentiation. Curr Opin Genet Dev. 1997;7(5):597–602. doi:10.1016/S0959-437X(97)80005-6 [PubMed: 9388774]
27. Ruijtenberg S, van den Heuvel S. Coordinating cell proliferation and differentiation: Antagonism between cell cycle regulators and cell type-specific gene expression. Cell Cycle. 2016;15(2):196–212. doi:10.1080/15384101.2015.1120925 [PubMed: 26825227]
28. Rochlin K, Yu S, Roy S, Baylies MK. Myoblast fusion: when it takes more to make one. Dev Biol. 2010;341(1):66–83. doi:10.1016/j.ydbio.2009.10.024 [PubMed: 19932206]
29. Chal J, Pourquié O. Making muscle: Skeletal myogenesis in vivo and in vitro. Development. 2017;144:2104–2122. doi:10.1242/dev.151035 [PubMed: 28634270]
30. Singh K, Dilworth FJ. Differential modulation of cell cycle progression distinguishes members of the myogenic regulatory factor family of transcription factors. FEBS J. 2013;280(17):3991–4003. doi:10.1111/febs.12188 [PubMed: 23419170]
31. Asfour HA, Allouh MZ, Said RS. Myogenic regulatory factors: The orchestrators of myogenesis after 30 years of discovery. Exp Biol Med. 2018;243(2):118–128. doi:10.1177/1535370217749494
32. Hernández-Hernández JM, García-González EG, Brun CE, Rudnicki MA. The myogenic regulatory factors, determinants of muscle development, cell identity and regeneration. Semin Cell Dev Biol. 2017. doi:10.1016/j.semcdb.2017.11.010
33. Zhang K, Sha J, Harter ML. Activation of Cdc6 by MyoD is associated with the expansion of quiescent myogenic satellite cells. J Cell Biol. 2010;188(1):39–48. doi:10.1083/jcb.200904144 [PubMed: 20048262]
34. Liu QC, Zha XH, Faralli H, et al. Comparative expression profiling identifies differential roles for Myogenin and p38α MAPK signaling in myogenesis. J Mol Cell Biol. 2012;4(6):386–397. doi:10.1093/jmcb/mjs045 [PubMed: 22847234]
35. Lee EJ, Malik A, Pokharel S, et al. Identification of genes differentially expressed in Myogenin knockdown bovine muscle satellite cells during differentiation through RNA sequencing analysis. PLoS One. 2014;9(3). doi:10.1371/journal.pone.0092447

36. Blais A, Tsikitis M, Acosta-Alvear D, Sharan R, Kluger Y, Dynlacht BD. An initial blueprint for myogenic differentiation. Genes Dev. 2005;19(5):553–569. doi:10.1101/gad.1281105 [PubMed: 15706034]
37. Zhang W, Liu Y, Zhang H. Extracellular matrix: an important regulator of cell functions and skeletal muscle development. Cell Biosci. 2021;11(1):1–13. doi:10.1186/s13578-021-00579-4 [PubMed: 33407894]
38. Gillies AR, Lieber RL. Structure and function of the skeletal muscle extracellular matrix. Muscle and Nerve. 2011;44(3):318–331. doi:10.1002/mus.22094 [PubMed: 21949456]
39. Thorsteinsdóttir S, Deries M, Cachaço AS, Bajanca F. The extracellular matrix dimension of skeletal muscle development. Dev Biol. 2011;354(2):191–207. doi:10.1016/j.ydbio.2011.03.015 [PubMed: 21420400]
40. Liu X, Gao Y, Long X, et al. Type i collagen promotes the migration and myogenic differentiation of C2C12 myoblasts: Via the release of interleukin-6 mediated by FAK/NF-κB p65 activation. Food Funct. 2020;11(1):328–338. doi:10.1039/c9fo01346f [PubMed: 31799535]
41. Henningsen J, Rigbolt KTG, Blagoev B, Pedersen BK, Kratchmarova I. Dynamics of the skeletal muscle secretome during myoblast differentiation. Mol Cell Proteomics. 2010;9(11):2482–2496. doi:10.1074/mcp.M110.002113 [PubMed: 20631206]
42. Giudice J, Taylor JM. Muscle as a paracrine and endocrine organ. Curr Opin Pharmacol. 2017;34:49–55. doi:10.1016/j.coph.2017.05.005 [PubMed: 28605657]
43. Pedersen BK, Febbraio MA. Muscles, exercise and obesity: Skeletal muscle as a secretory organ. Nat Rev Endocrinol. 2012;8(8):457–465. doi:10.1038/nrendo.2012.49 [PubMed: 22473333]
44. Florin A, Lambert C, Sanchez C, et al. The secretome of skeletal muscle cells: A systematic review. Osteoarthr Cartil Open. 2020;2(1):100019. doi:10.1016/j.ocarto.2019.100019 [PubMed: 36474563]
45. Murphy DP, Nicholson T, Jones SW, O'Leary MF. MyoCount: A software tool for the automated quantification of myotube surface area and nuclear fusion index. Wellcome Open Res. 2019;4(6). doi:10.12688/wellcomeopenres.15055.1
46. Tyanova S, Temu T, Sinitcyn P, et al. The Perseus computational platform for comprehensive analysis of (prote)omics data. Nat Methods. 2016;13(9):731–740. doi:10.1038/nmeth.3901 [PubMed: 27348712]
47. Giudice J, Xia Z, Wang ET, et al. Alternative splicing regulates vesicular trafficking genes in cardiomyocytes during postnatal heart development. Nat Commun. 2014;5:1–15. doi:10.1038/ncomms4603
48. Giudice J, Loehr JA, Rodney GG, Cooper TA. Alternative splicing of four trafficking genes regulates myofiber structure and skeletal muscle physiology. Cell Rep. 2016;17(8):1923–1933. doi:10.1016/j.celrep.2016.10.072 [PubMed: 27851958]
49. Panda AC, Abdelmohsen K, Martindale JL, et al. Novel RNA-binding activity of MYF5 enhances Ccnd1/Cyclin D1 mRNA translation during myogenesis. Nucleic Acids Res. 2016;44(5):2393–2408. doi:10.1093/nar/gkw023 [PubMed: 26819411]
50. Rao SS, Chu C, Kohtz DS. Ectopic expression of cyclin D1 prevents activation of gene transcription by myogenic basic helix-loop-helix regulators. Mol Cell Biol. 1994;14(8):5259–5267. doi:10.1128/mcb.14.8.5259 [PubMed: 8035804]
51. Chan XCY, McDermott JC, Siu KWM. Identification of secreted proteins during skeletal muscle development. J Proteome Res. 2007;6(2):698–710. doi:10.1021/pr060448k [PubMed: 17269726]
52. Grube L, Dellen R, Kruse F, Schwender H, Stühler K, Poschmann G. Mining the Secretome of C2C12 Muscle Cells: Data Dependent Experimental Approach to Analyze Protein Secretion Using Label-Free Quantification and Peptide Based Analysis. J Proteome Res. 2018;17(2):879–890. doi:10.1021/acs.jproteome.7b00684 [PubMed: 29322779]
53. Ahmad SS, Ahmad K, Lee EJ, Lee YH, Choi I. Implications of insulin-like growth factor-1 in skeletal muscle and various diseases. Cells. 2020;9(8):107–115. doi:10.3390/cells9081773 [PubMed: 31906296]
54. Grassi D, Plonka FB, Oksdath M, Guil AN, Sosa LJ, Quiroga S. Selected SNARE proteins are essential for the polarized membrane insertion of igf-1 receptor and the regulation of initial

axonal outgrowth in neurons. Cell Discov. 2015;1:15023. doi:10.1038/celldisc.2015.23 [PubMed: 27462422]

55. Gérard C, Goldbeter A. The balance between cell cycle arrest and cell proliferation: Control by the extracellular matrix and by contact inhibition. Interface Focus. 2014;4(3). doi:10.1098/rsfs.2013.0075
56. Tanaka K, Sato K, Yoshida T, et al. Evidence for cell density affecting C2C12 myogenesis: Possible regulation of myogenesis by cell-cell communication. Muscle and Nerve. 2011;44(6):968–977. doi:10.1002/mus.22224 [PubMed: 22102468]
57. Chowdhury SR, Muneyuki Y, Takezawa Y, et al. Growth and differentiation potentials in confluent state of culture of human skeletal muscle myoblasts. J Biosci Bioeng. 2010;109(3):310–313. doi:10.1016/j.jbiosc.2009.09.042 [PubMed: 20159584]
58. Kaspar P, Pajer P, Sedlak D, Tamaoki T, Dvorak M. c-Myb inhibits myogenic differentiation through repression of MyoD. Exp Cell Res. 2005;309(2):419–428. doi:10.1016/j.yexcr.2005.06.016 [PubMed: 16055116]
59. Lindon C, Albagli O, Pinset C, Montarras D. Cell density-dependent induction of endogenous myogenin (myf4) gene expression by Myf5. Dev Biol. 2001;240(2):574–584. doi:10.1006/dbio.2001.0435 [PubMed: 11784084]
60. Stallaert W, Kedziora KM, Taylor CD, et al. The structure of the human cell cycle. Cell Syst. 2022;13(3):230–240.e3. doi:10.1016/j.cels.2021.10.007 [PubMed: 34800361]
61. Fusté NP, Fernández-Hernández R, Cemeli T, et al. Cytoplasmic cyclin D1 regulates cell invasion and metastasis through the phosphorylation of paxillin. Nat Commun. 2016;7(1):11581. doi:10.1038/ncomms11581 [PubMed: 27181366]
62. Neumeister P, Pixley FJ, Xiong Y, et al. Cyclin D1 Governs Adhesion and Motility of Macrophages. Mol Biol Cell. 2003;14(5):2005–2015. doi:10.1091/mbc.02-07-0102 [PubMed: 12802071]
63. Li Z, Wang C, Prendergast G, Pestell RG. Cyclin D1 Functions in Cell Migration. Cell Cycle. 2006;5(21):2440–2442. doi:10.4161/cc.5.21.3428 [PubMed: 17106256]
64. Zhiping L, Chenguang W, Xuanmao J, et al. Cyclin D1 Regulates Cellular Migration through the Inhibition of Thrombospondin 1 and ROCK Signaling. Mol Cell Biol. 2006;26(11):4240–4256. doi:10.1128/MCB.02124-05 [PubMed: 16705174]
65. Zhang JM, Wei Q, Zhao X, Paterson BM. Coupling of the cell cycle and myogenesis through the cyclin D1-dependent interaction of MyoD with cdk4. EMBO J. 1999;18(4):926–933. doi:10.1093/emboj/18.4.926 [PubMed: 10022835]
66. Skapek SX, Rhee J, Spicer DB, Lassar AB. Inhibition of myogenic differentiation in proliferating myoblasts by cyclin D1-dependent kinase. Science (80-). 1995;267:1022–1024. doi:10.1126/science.7863328
67. Zhang JM, Zhao X, Wei Q, Paterson BM. Direct inhibition of G1 cdk kinase activity by MyoD promotes myoblast cell cycle withdrawal and terminal differentiation. EMBO J. 1999;18(24):6983–6993. doi:10.1093/emboj/18.24.6983 [PubMed: 10601020]
68. Kitzmann M, Carnac G, Vandromme M, Primig M, Lamb NJC, Fernandez A. The muscle regulatory factors MyoD and Myf-5 undergo distinct cell cycle-specific expression in muscle cells. J Cell Biol. 1998;142(6):1447–1459. doi:10.1083/jcb.142.6.1447 [PubMed: 9744876]
69. Kitzmann M, Fernandez A. Crosstalk between cell cycle regulators and the myogenic factor MyoD in skeletal myoblasts. Cell Mol Life Sci C. 2001;58(4):571–579. doi:10.1007/PL00000882
70. Tollefsen SE, Lajara R, McCusker RH, Clemmons DR, Rotwein P. Insulin-like Growth Factors (IGF) in Muscle Development: Expression of IGF-I, the IGF-I receptor, and an IGF Binding Protein During Myoblast Differentiation. J Biol Chem. 1989;264(23):13810–13817. doi:10.1016/S0021-9258(18)80073-4 [PubMed: 2474537]
71. Engert JC, Berglund EB, Rosenthal N. Proliferation precedes differentiation in IGF-I-stimulated myogenesis. J Cell Biol. 1996;153(2):431–440. doi:10.1083/jcb.135.2.431
72. Florini JR, Ewton DZ, Roof SL. Insulin-Like Growth Factor-I Stimulates Terminal Myogenic Differentiation by Induction of Myogenin Gene Expression. Mol Endocrinol. 1991;5(5):718–724. doi:10.1210/mend-5-5-718 [PubMed: 1649394]

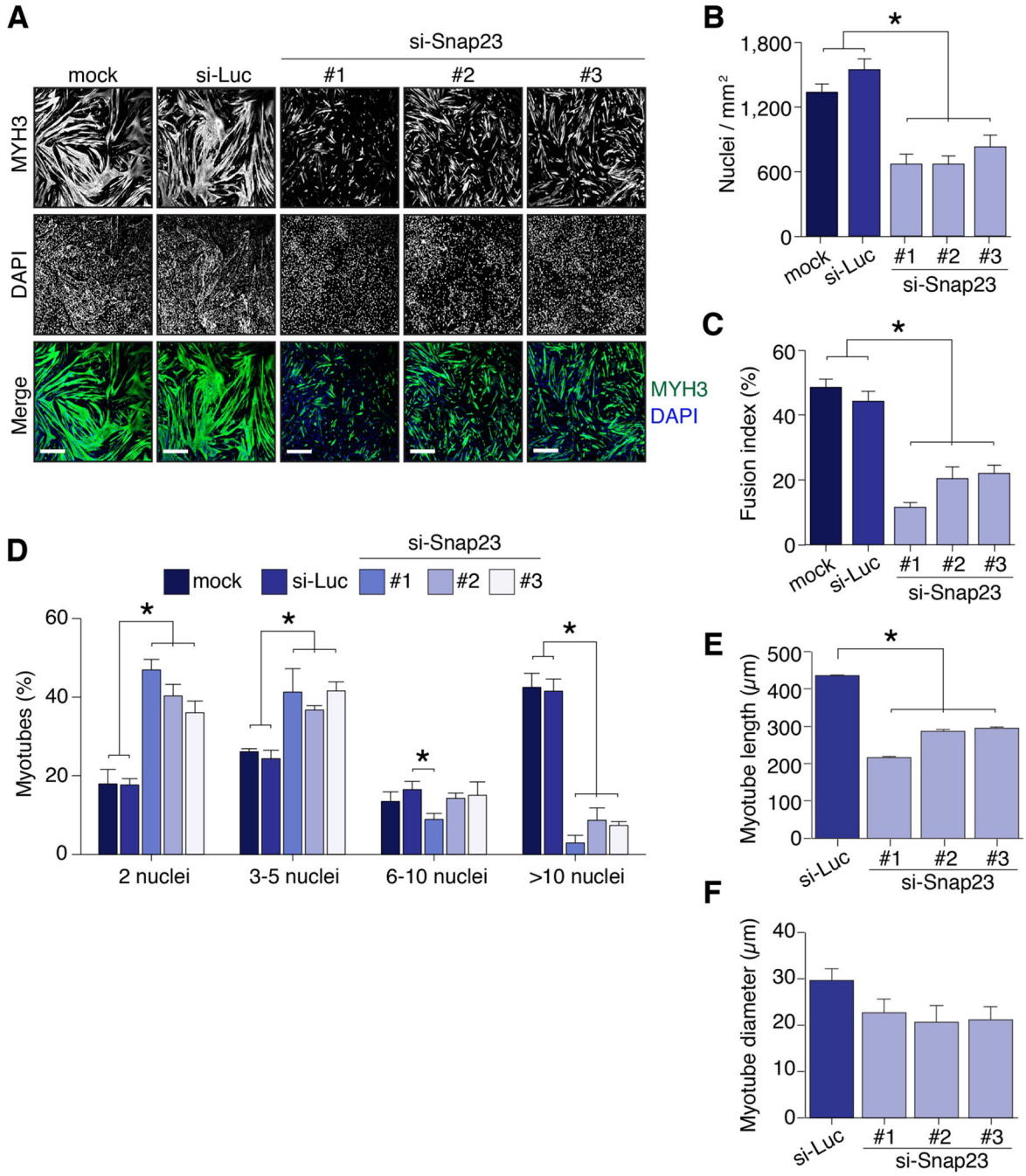

Figure 1. SNAP23 is necessary for myogenesis.

C2C12 myoblasts were transfected with a control si-Luciferase (si-Luc) or one of three different si-RNAs targeting Snap23 (#1, #2, and #3). The next day, cells were differentiated for four to five days. **A.** Immunofluorescence assays were performed to analyze expression of myosin heavy chain 3 (MYH3) and thus muscle cell differentiation. Scale bars: 500 μm. **B-F.** The number of nuclei per unit area (**B**), the fusion index (**C**), the distribution of myotubes with different number of nuclei (**D**), the myotube length (**E**), and the myotube diameter (**F**) were estimated from the immunofluorescence experiments using ImageJ

software. Results are shown as the mean ± SEM, *$p \leq 0.05$ *versus* mock and si-Luc, one-way ANOVA with Bonferroni post hoc test for multiple comparisons for panels **B** and **C**, MANOVA test for panel **D**, and Student's T-test for panels **E** and **F**, $n = 12$ (panels **B-C**), and $n = 4$ (panel **D-F**) independent experiments.

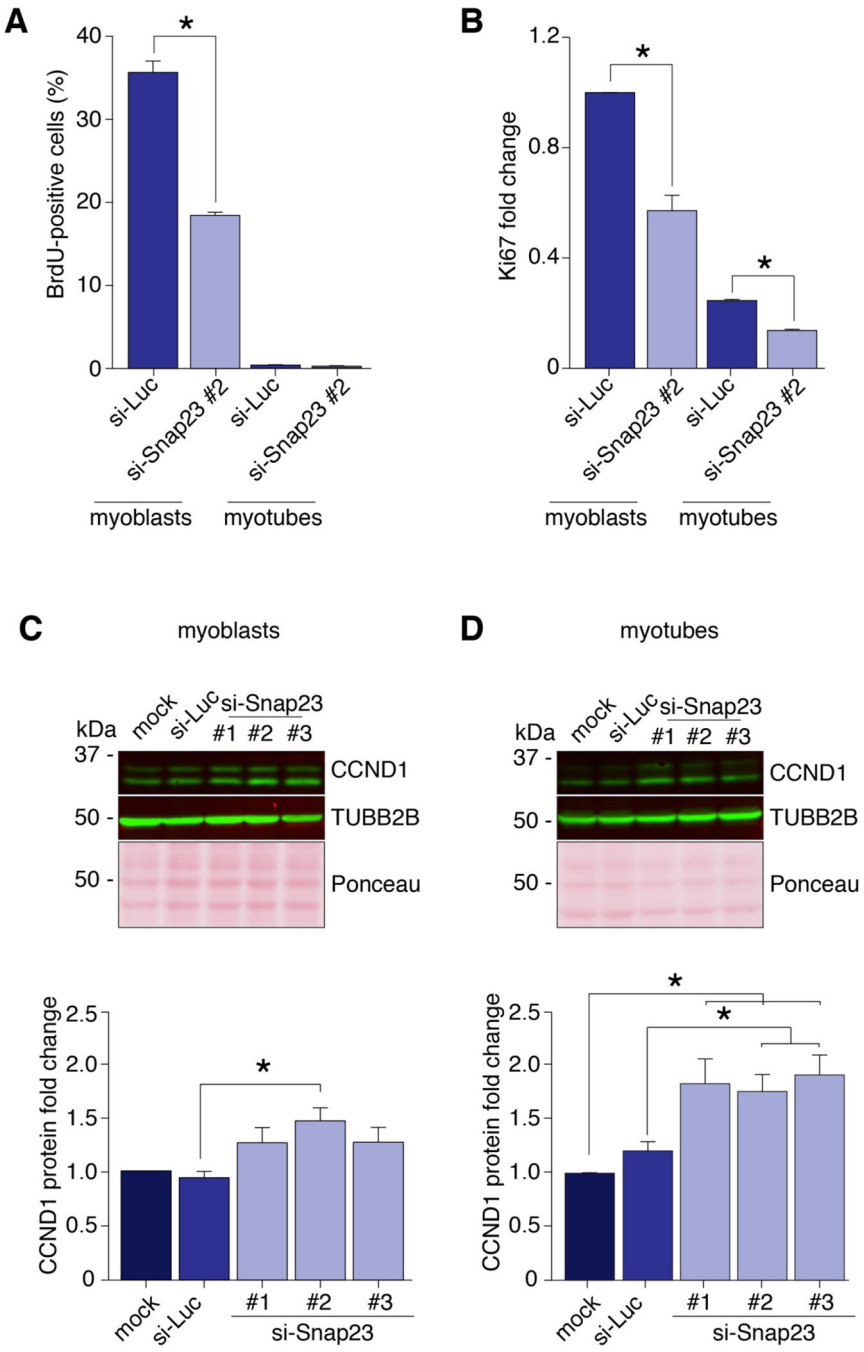

Figure 2. SNAP23 depletion decreases myoblast proliferation.

C2C12 myoblasts were transfected with a control si-Luciferase (si-Luc) or one of three different si-RNAs targeting Snap23 (#1, #2, and #3). **A.** Myoblasts and myotubes were treated with BrdU and immunofluorescence assays were performed to calculate the percentage of proliferating (*i.e.*, Brdu-positive) cells. **B.** The expression of Ki67 was measured by qPCR in myoblasts and myotubes. **C-D.** The expression of cyclin D1 (CCND1) was measured by western blot experiments in myoblasts (**C**) and myotubes (**D**). Results are shown as the mean ± SEM, $*p \leq 0.05$ *versus* mock and si-Luc, Student's T-test for panels **A**

and **B**, one-way ANOVA with Bonferroni post hoc test for multiple comparisons for panels **C** and **D**, $n = 3–5$ independent experiments. TUBB2B: beta-tubulin.

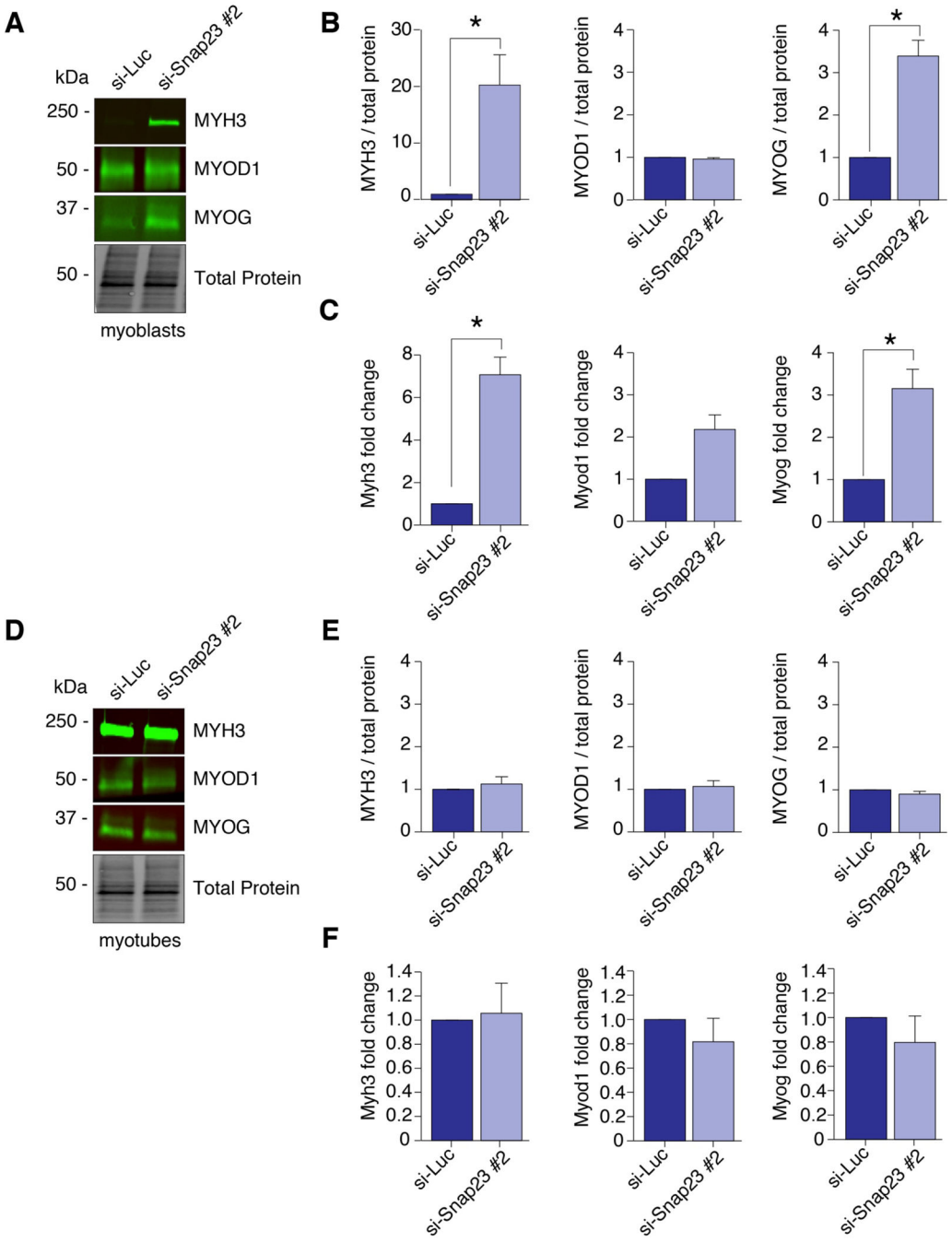

Figure 3. SNAP23 depletion activates myogenic marker expression in myoblasts.

C2C12 myoblasts were transfected with a control si-Luciferase (si-Luc) or si-RNA targeting Snap23 (#2). **A-C.** Myoblasts were analyzed for expression of myosin heavy chain 3 (MYH3), myoblast determination protein 1 (MYOD1), and myogenin (MYOG) by western blot (**A-B**) and qPCR (**C**) assays. **D-F.** Myotubes were analyzed for expression of myosin heavy chain 3 (MYH3), myoblast determination protein 1 (MYOD1), and myogenin (MYOG) by western blot (**D-E**) and qPCR (**F**). Results are shown as the mean ± SEM, $*p \leq 0.05$ *versus* si-Luc, Student's T-test, $n = 3$ independent experiments.

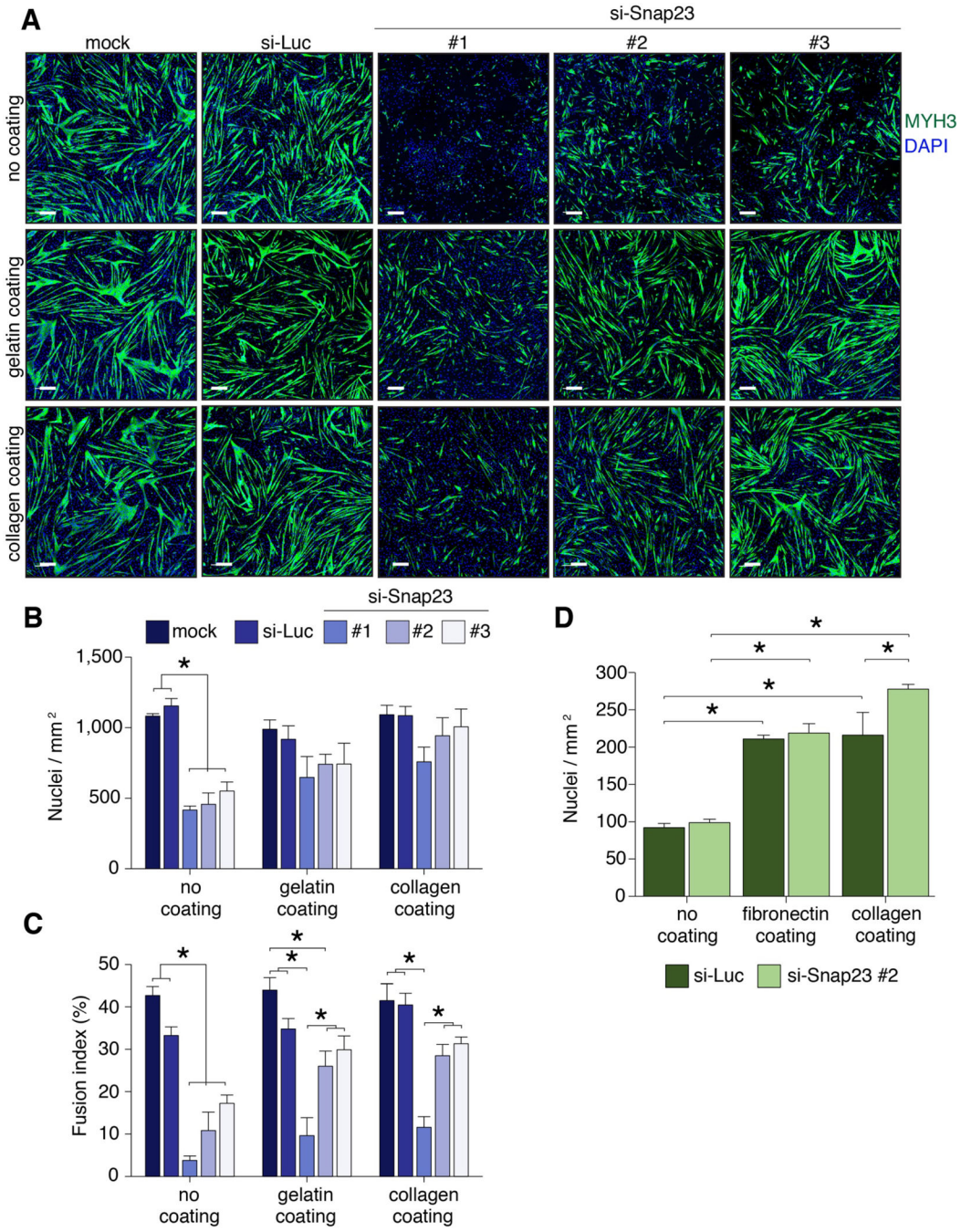

Figure 4. Collagen or gelatin coating rescues total nuclei and fusion after SNAP23 depletion.

A-C. C2C12 myoblasts were plated either on non-coated plates or on plates coated with gelatin or collagen. The next day, cells were transfected with a control si-Luciferase (si-Luc) or one of three different si-RNAs targeting Snap23 (#1, #2, and #3). After 24h, differentiation was induced for five days. Expression of myosin heavy chain 3 (MYH3) was analyzed by immunofluorescence (**A**). Scale bars: 200 μm. The total number of nuclei per unit area (**B**) and the fusion index (**C**) were estimated from the immunofluorescence experiments using ImageJ software. **D.** C2C12 myoblasts were transfected with a control

si-Luciferase (si-Luc) or si-RNA targeting Snap23 (#2). Transfected cells were then seeded on plates coated with fibronectin or collagen. The number of adhered cells was estimated by calculating the total nuclei per unit area. Results are shown as the mean ± SEM, $*p < 0.05$, two-way ANOVA with Bonferroni post hoc test for multiple comparisons, $n = 3–6$ independent experiments.

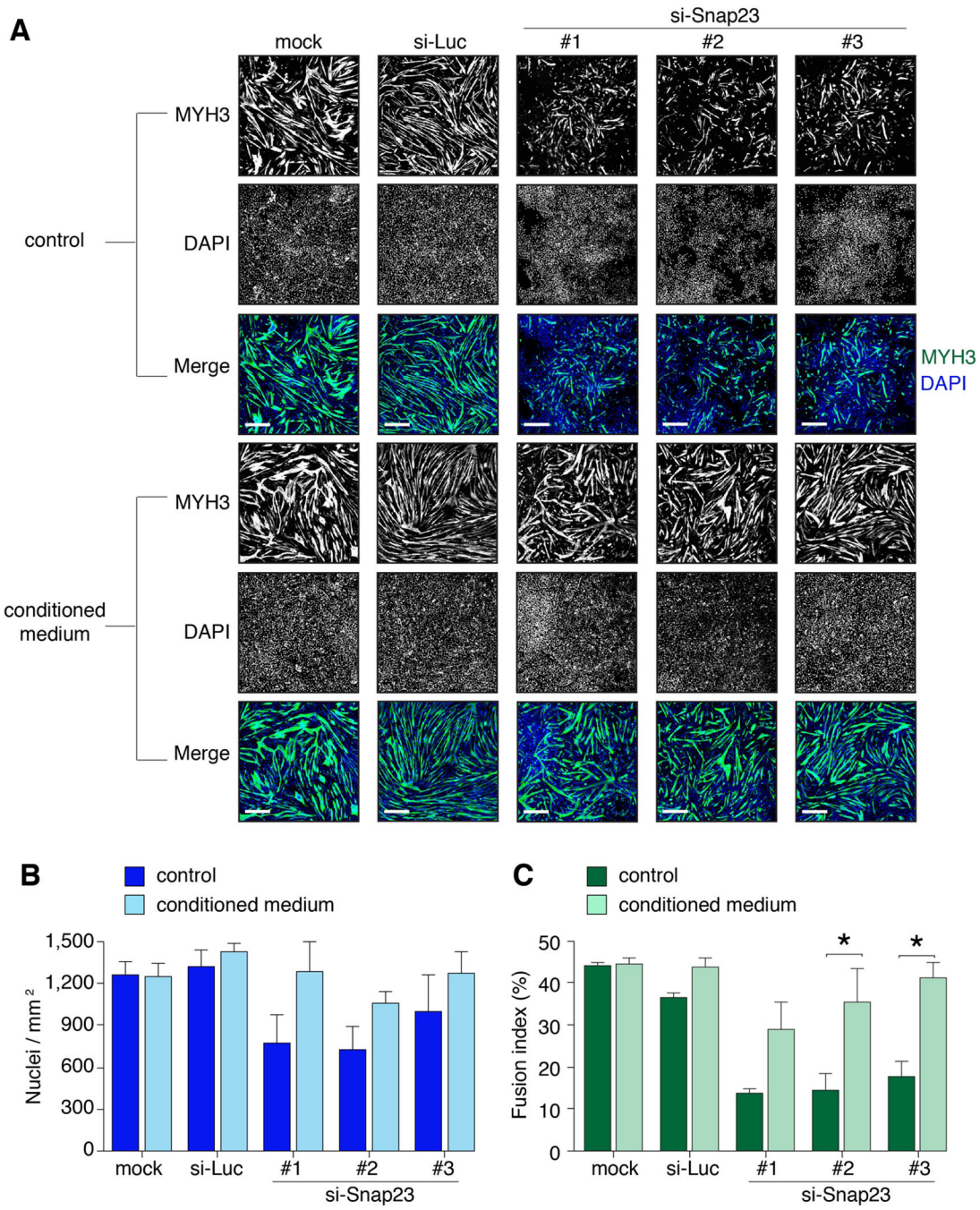

Figure 5. SNAP23 mediates the secretion of factors that are necessary for myogenesis.

C2C12 myoblasts were transfected with a control si-Luciferase (si-Luc) or one of three different si-RNAs targeting Snap23 (#1, #2, and #3). The next day, cells were differentiated for five to six days in standard (control) or conditioned differentiation culture medium. **A.** Expression of myosin heavy chain 3 (MYH3) was analyzed by immunofluorescence. Scale bars: 500 μm. **B-C.** The total number of nuclei per unit area (**B**) and the fusion index (**C**) were estimated from the immunofluorescence experiments using ImageJ software. Results are shown as the mean ± SEM, *$p < 0.05$ *versus* the standard differentiation culture medium

(control), two-way ANOVA with Bonferroni post hoc test for multiple comparisons, $n = 5$ independent experiments.

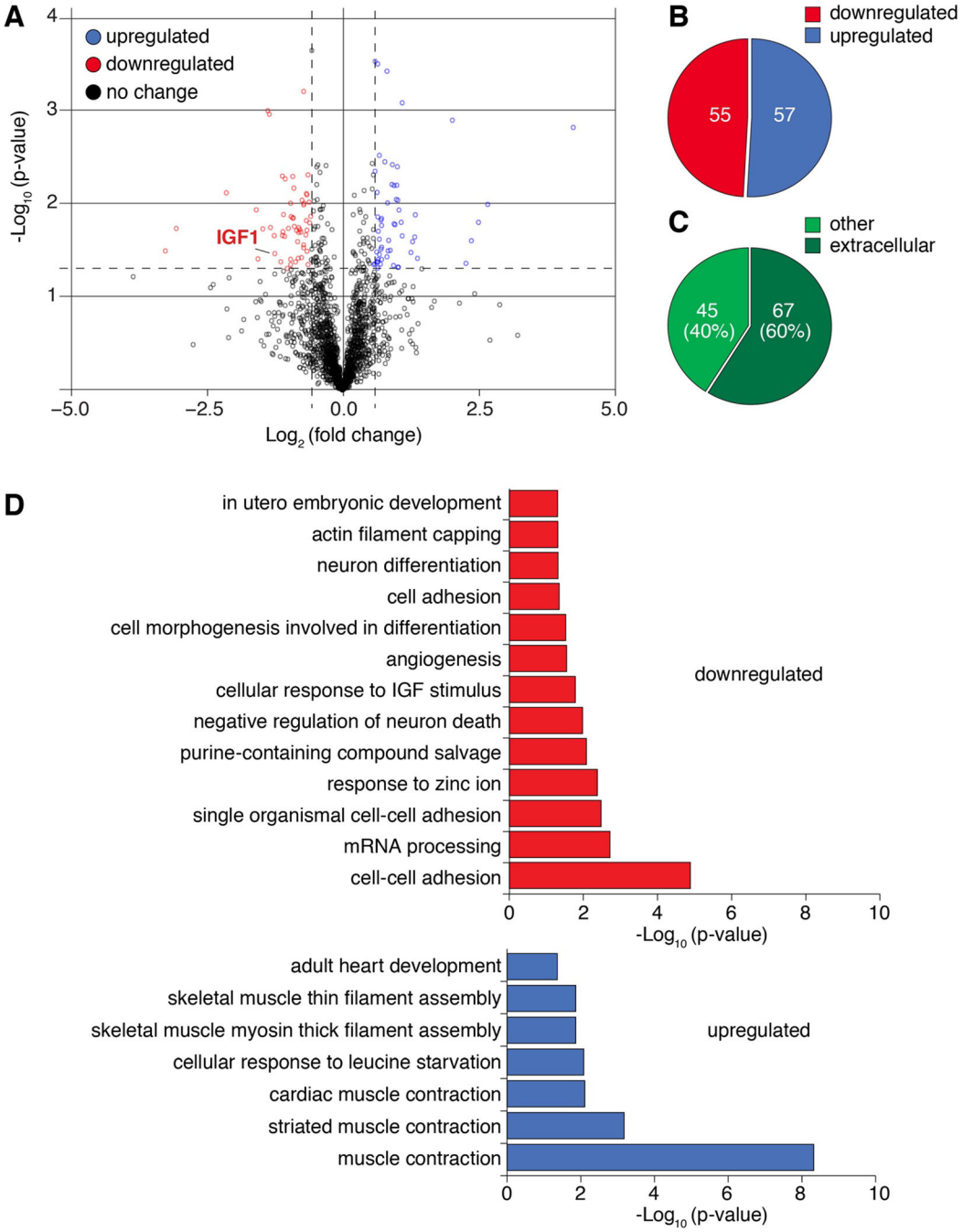

Figure 6. Loss of SNAP23 alters the secretome profile of muscle cells.

A. Volcano plot of the proteomics data comparing the secretome of SNAP23-depleted cells to control cells. Thresholds were applied for significance (horizontal dashed line) and differential expression (vertical dashed lines). **B.** Total number of upregulated and downregulated secreted proteins meeting the threshold criteria. “Upregulated” refers to proteins more abundant in the medium collected from SNAP23-depleted cells than in controls. “Downregulated” refers to proteins less abundant in the medium collected from SNAP23-depleted cells than in controls. **C.** Distribution of the differentially secreted

proteins that are known to be residents of the extracellular space. **D.** GO analysis on the differentially secreted proteins. Proteomics studies were performed in triplicate, $n = 3$ independent experiments.

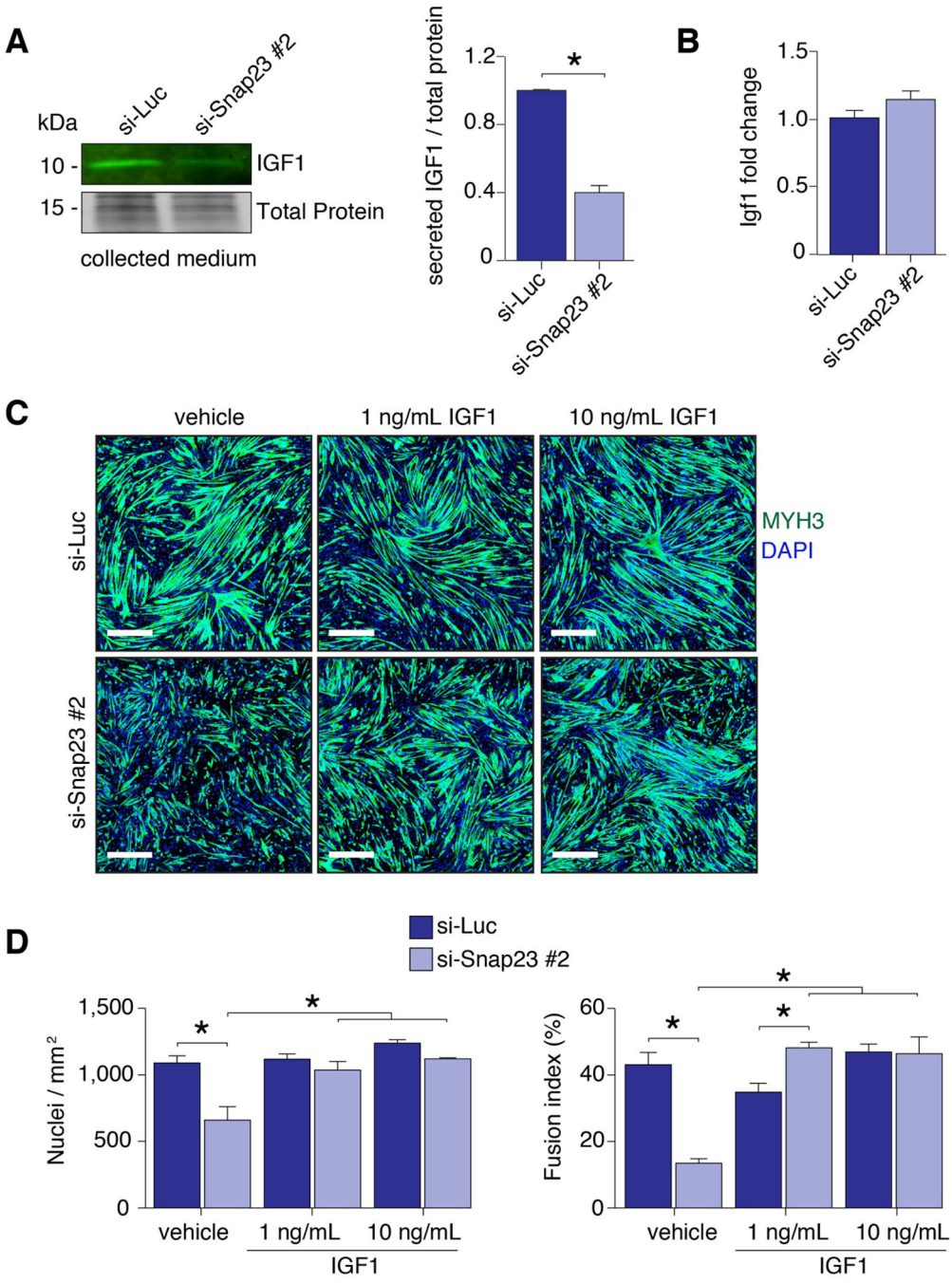

Figure 7. SNAP23-mediated secretion of IGF1 is important for myogenesis.

C2C12 myoblasts were transfected with a control si-Luciferase (si-Luc) or si-RNA targeting Snap23 (#2). After 24h, differentiation was induced for six days. Medium was collected at day four and six of differentiation. **A.** Western blot validation and quantification of secreted IGF1. **B.** qPCR of total Igf1 mRNA abundance in myotubes. **C.** Immunofluorescence images staining for myosin heavy chain 3 (MYH3) in control (si-Luc) or SNAP23-depleted (si-Snap23 #2) cells in the presence or absence of exogenous IGF1 treatment at two different concentrations. Scale bars: 500 μm. **D.** The total number of nuclei per unit area and the

fusion index were estimated from the immunofluorescence images using MyoCount. Results are shown as the mean ± SEM, $*p \leq 0.05$ *versus* si-Luc, two-way ANOVA with Bonferroni post hoc test for multiple comparisons, $n = 3–4$ independent experiments.